



# **Open Access Research Article**



# An ITO thermochromic hydrogel-based smart window for balancing indoor daylight comfort and energy regulation

Zhucheng Jiang<sup>1</sup>, Yanzhao Yang<sup>2,\*</sup>, Yu Li<sup>1</sup>, Cong Peng<sup>1</sup>, Wei Feng<sup>1,2,\*</sup>

\*Correspondence to: Yanzhao Yang, School of Materials Science and Engineering, Tianjin University, Tianjin 300350, China. E-mail: yangyanzhao@tju.edu.cn

Wei Feng, School of Materials Science and Engineering, Tianjin University, Tianjin 300350, China. E-mail: weifeng@tju.edu.cn

Received: August 22, 2025 Accepted: September 18, 2025 Published: September 19, 2025

**Cite this article:** Jiang Z, Yang Y, Li Y, Peng C, Feng W. An ITO thermochromic hydrogel-based smart window for balancing indoor daylight comfort and energy regulation. Thermo-X. 2025;1:202504. https://doi.org/10.70401/tx.2025.0003

#### **Abstract**

Enhancing indoor visual comfort is crucial for the practical deployment of thermochromic smart windows. However, their application is often hindered by the low visible light transmittance ( $T_{lum}$ ) in the activated state. In this study, we propose a thermally and optically dual-responsive smart window that improves both building energy efficiency and  $T_{lum}$  in the activated state. The design is based on a polyacrylamide (PAm)/poly(N-isopropylacrylamide) (PNIPAm)/indium tin oxide (ITO) composite film (PPI). Within this structure, PAm provides a hydrophilic matrix, PNIPAm microgels enable thermoresponsive optical modulation through reversible transmittance changes across the response temperature, and ITO particles act as light-to-heat transducers due to their photothermal and infrared reflective properties. Compared with the PNIPAm hydrogel film, the PPI composite film increases  $T_{lum}$  in the activated state from 9.7% to 50.0% and enhances infrared modulation capability from 39.2% to 50.4%. Under an illumination intensity of 95 mW cm<sup>-2</sup>, the PPI composite film lowers the indoor temperature of simulated buildings by up to 7 °C. This dual-responsive thermochromic window provides improved indoor visual comfort along with effective temperature regulation, offering a promising strategy for advancing the practical use of smart windows.

Keywords: Smart window, PNIPAm, ITO, selective transmittance, dual-responsive

### 1. Introduction

Building energy consumption accounts for approximately 40% of global energy use, surpassing the combined consumption of the industrial and transportation sectors. More than half of this energy is expended on heating, ventilation, and air conditioning systems<sup>[1-4]</sup>. Consequently, enhancing building energy efficiency has become an urgent priority, drawing increasing attention to the development of smart thermal management materials<sup>[5,6]</sup>. Among these, thermochromic smart windows, particularly those based on poly(N-isopropylacrylamide) (PNIPAm), have attracted significant interest because of their ability to regulate solar heat gain in response to temperature fluctuations<sup>[7,8]</sup>. For an ideal smart window, it is critical to achieve a substantial difference in solar energy transmission at temperatures above and below the response temperature ( $T_c$ ), thereby enabling effective solar energy modulation  $(\Delta T_{sol})$ . At the same time, the window must maintain high visible light transmittance ( $T_{lum}$ ) in the activated state remains a considerable challenge.

Conventional PNIPAm-based systems often show a trade-off between these parameters, as increasing  $\Delta T_{sol}$  usually leads to a reduction in  $T_{lum}$ , which can compromise indoor visual comfort, a factor that directly affects occupant well-being and productivity<sup>[10-12]</sup>. To address this issue, Fang *et al.* enhanced the infrared modulation capability ( $\Delta T_{IR}$ ) and reduced visible light blocking by tuning the size of PNIPAm/2-aminoethylmethacrylate hydrochloride microparticles, achieving an overall  $\Delta T_{sol}$  of 81.3%<sup>[13]</sup>. Zhou *et al.* investigated the influence of PNIPAm film thickness on smart window performance and reported that thinner films improve  $T_{lum}$  in the activated state<sup>[14]</sup>. However, this approach also increases infrared transmittance ( $T_{IR}$ ), which diminishes overall effectiveness. Yang *et al.* integrated antimony-doped tin oxide nanocrystals with different levels of fluorine doping into a poly(N-isopropylacrylamide)-chitosan hydrogel, resulting in a prototype smart window with rapid photothermal response, high visible light transmittance, and excellent near-infrared shielding performance<sup>[15]</sup>. Although these advances have considerably improved PNIPAm-based smart window technologies, achieving a balance between high  $\Delta T_{sol}$  and high  $T_{lum}$  in the activated state

#### remains a significant challenge.

In this study, we introduce a dual-responsive polyacrylamide/PNIPAm/indium tin oxide (PPI) composite film, in which PNIPAm microgels and indium tin oxide (ITO) particles are incorporated into a polyacrylamide (PAm) hydrogel matrix. This design achieves a high Tlum in the activated state while simultaneously enhancing  $\Delta T_{IR}$ . As illustrated in Figure 1, ITO, a transparent conductive oxide, exploits its infrared reflectance and photothermal properties to improve infrared modulation and provide light-responsive functionality, even though its primary applications lie in other technological fields<sup>[16-18]</sup>. The PNIPAm microgels undergo reversible transmittance changes across the  $T_{C}$ , enabling thermally driven optical modulation, whereas PAm serves as a hydrophilic and mechanically stable framework. Consequently, the PPI composite film exhibits a balanced performance profile by combining high  $T_{lum}$  in the activated state with enhanced  $\Delta T_{IR}$  compared with conventional PNIPAm systems. Under an illumination intensity of 95 mW cm<sup>-2</sup>, the composite film reduced the indoor temperature of simulated buildings by up to 7 °C. These results highlight a practical strategy to overcome the  $\Delta T_{sol}$ - $T_{lum}$  trade-off and demonstrate the potential of PNIPAm-based smart windows for integration into energy-efficient building systems.

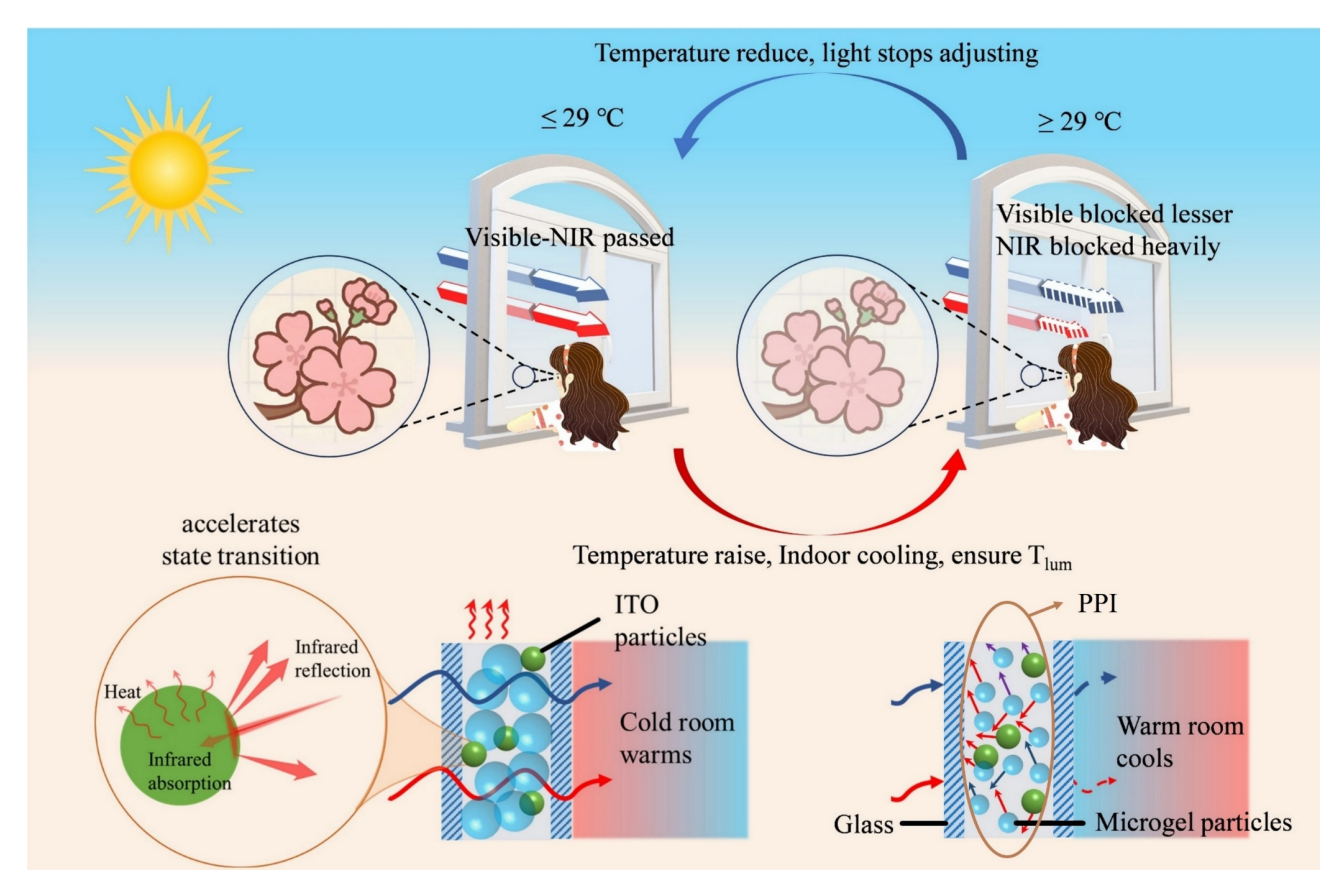


Figure 1. The working mechanism of the PPI composite film in this work. PPI: polyacrylamide/poly(N-isopropylacrylamide)/indium tin oxide. The working mechanism of the PPI composite film in this work. PPI: polyacrylamide/poly(N-isopropylacrylamide)/indium tin oxide. The working mechanism of the PPI composite film in this work. PPI: polyacrylamide/poly(N-isopropylacrylamide)/indium tin oxide. The working mechanism of the PPI composite film in this work. PPI: polyacrylamide/poly(N-isopropylacrylamide)/indium tin oxide. The working mechanism of the PPI composite film in this work. PPI: polyacrylamide/poly(N-isopropylacrylamide)/indium tin oxide. The working mechanism is a simple film of the PPI composite film in this work. The working mechanism is a simple film oxide. The working mechanism is

## 2. Experimental Section

#### 2.1 Materials

N-isopropylacrylamide (NIPAm, 98%), ammonium persulfate (APS, 99.99%) initiator, and acrylamide (Am, 99%) were purchased from Shanghai Macklin Biochemical Co., Ltd. (Shanghai, China). N, N'-methylenebis(acrylamide) (BIS, 99%) crosslinker, N, N, N', N'-tetramethylethylenediamine (TEMED, 99%) catalyst, and sodium dodecyl sulfate (SDS, 98.5%) surfactant were obtained from Shanghai Aladdin Biochemical Technology Co., Ltd. (Shanghai, China). Indium tin oxide (ITO, 50nm) particles were supplied by Suzhou Youyan New Material Industry Co., Ltd. (Suzhou, China).

## 2.2 Synthesis of PNIPAm Microparticles

PNIPAm microparticles were synthesized via continuous feeding of NIPAm into the reaction vessel. Solution A was prepared by dissolving 1g of NIPAm and 12mg of BIS in 15mL of deionized (DI) water, while Solution B was prepared by dissolving 7g of NIPAm and 168mg of BIS in 25mL of DI water. SDS and APS stock solutions were prepared at concentrations of 0.19M and 0.36M, respectively. Subsequently, 5mL of Solution A and 0.76mL of 0.19M SDS solution were added to 100mL of DI water in the reaction vessel, which was heated to 80 °C under a nitrogen atmosphere and stirred at 700rpm. Polymerization was initiated by adding 0.76mL of 0.36M APS

solution. After 1min, Solution B was introduced into the reaction vessel using a syringe pump at a constant feed rate of 200  $\mu$ L min<sup>-1</sup>. The particle size of the resulting PNIPAm microparticles could be precisely controlled by adjusting the total feeding duration. Upon completion, a stable dispersion of PNIPAm microparticles was obtained.

## 2.3 Preparation of PPI hydrogel film

The PAm-PNIPAm (P-P) composite film was prepared using the PNIPAm microparticle dispersion. Am (2g), BIS (6mg), and APS (10mg) were dissolved in 10mL of the microparticle dispersion under continuous stirring in an ice-water bath until fully dissolved. Subsequently,  $50~\mu$ L of TEMED was added, followed by stirring for 1min. The resulting mixture was immediately poured into a glass mold, with film thickness controlled by adjusting the spacing between the glass plates. The mold was left undisturbed for 24 h, yielding composite hydrogel films of varying thicknesses. The PPI hydrogel film was prepared using the same procedure, with the addition of ITO particles into the mixture during the ice-water bath stage.

#### 2.4 Characterization

The crystal structure of the ITO particles was analyzed by XRD (SmartLab SE, Rigaku, Japan), and their morphology and particle size were examined using SEM (SU8600, Hitachi, Japan). The  $T_C$  of the hydrogel films was determined by differential scanning calorimetry (DSC, Q20, TA Instruments, USA). FTIR spectra were acquired using a Nicolet 6700 spectrometer (Thermo Scientific, USA). The photothermal properties of both the ITO particles and hydrogel films were evaluated using a photothermal heating system coupled with infrared thermal imaging. The transmittance of the ITO particles and hydrogel films was measured with an in situ UV-Vis-NIR spectrophotometer (Lambda 950, PerkinElmer, USA). Additionally, the size distribution of the hydrogel particles was analyzed by dynamic light scattering (DLS, Zetasizer Nano ZS90, Malvern Instruments, UK), and their morphology was further examined using an optical microscope (BX53, Olympus, Japan).

The integral luminous transmittance,  $T_{lum}$  (380-780 nm), IR transmittance,  $T_{IR}$  (780-2,500 nm), and solar transmittance,  $T_{sol}$  (220-2,500 nm) were calculated according to Eqn (1):

$$T_{\text{lum/IR/sol}} = \frac{\int \varphi_{\text{lum/IR/sol}}(\lambda) T(\lambda) d\lambda}{\int \varphi_{\text{lum/IR/sol}}(\lambda) d\lambda}$$
(1)

Where  $T(\lambda)$  denotes the spectral transmittance,  $\phi_{lum}(\lambda)$  is the standard luminous efficiency function for photopic vision in the wavelength range 380-780 nm, and  $\phi_{IR}(\lambda)$  and  $\phi_{sol}(\lambda)$  represent the infrared and solar irradiance spectra, respectively, for an air mass of 1.5 (corresponding to the sun at 37° above the horizon, with a solar zenith angle of 48.2°). The relative changes in transmittance,  $\Delta T_{lum/IR/sol}$  were calculated as follows:

$$\Delta T_{\text{lum/IR/sol}} = T_{\text{lum/IR/sol},20^{\circ}C} - T_{\text{lum/IR/sol},35^{\circ}C}$$
(2)

# 3. Results and Discussion

# 3.1 The fabrication of the composite film

The fabrication process of the composite film is illustrated in Figure 2. ITO particles were introduced into the smart window design with two objectives: (i) to significantly enhance  $\Delta T_{IR}$  and (ii) to improve the switching speed of the film. The structural and morphological characteristics of the ITO particles were first examined by X-ray diffraction (XRD) and scanning electron microscopy (SEM), as shown in Figure S1.

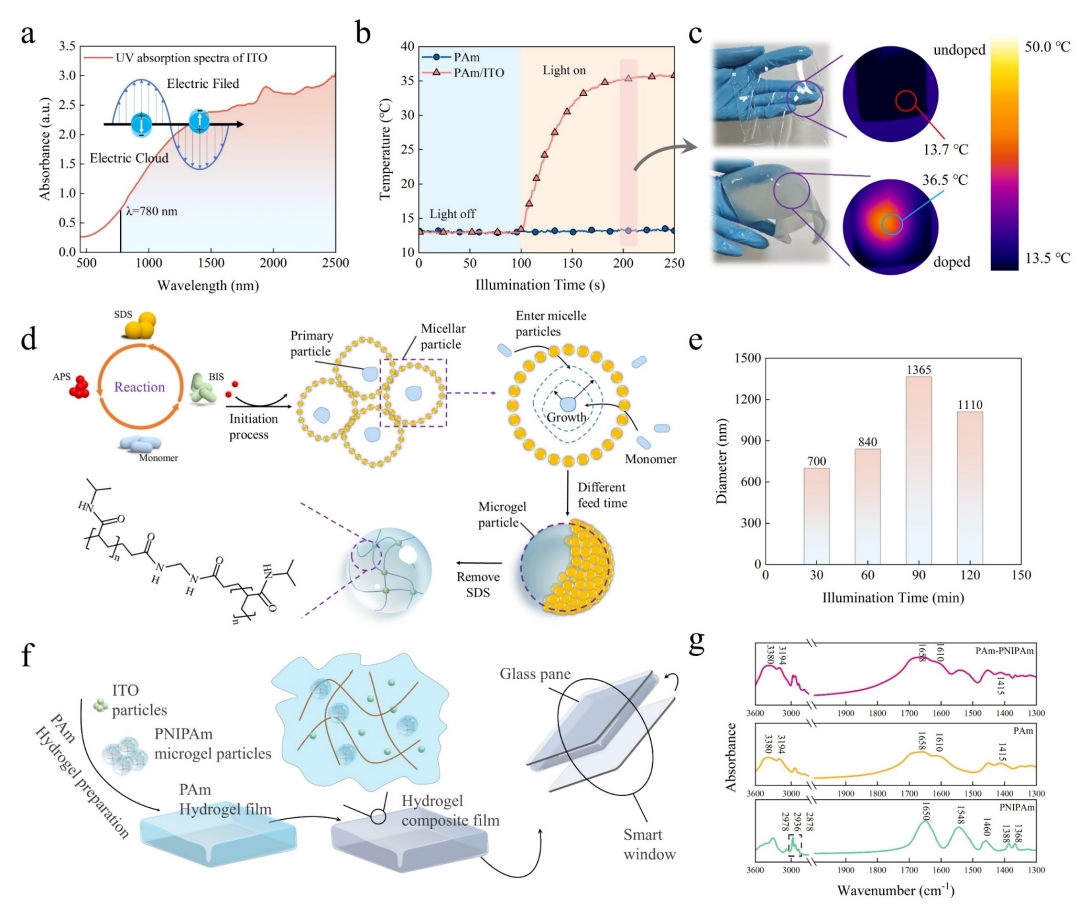


Figure 2. Characterization of ITO particles, PNIPAm microgels, and smart window films. (a) UV-vis spectrum of ITO particles; (b) Photothermal properties of ITO particles; (c) Infrared thermography of films shown in (b); (d) Continuous feeding method for PNIPAm synthesis; (e) Microgel size distribution at different feeding times; (f) Fabrication process of the smart window film. (g) FTIR spectrum of the hydrogel. ITO: indium tin oxide; PNIPAm: poly(N-isopropylacrylamide); FTIR: Fourier transform infrared spectroscopy.

As depicted in Figure 2a, the particles exhibit strong absorption in the near-infrared region, which is primarily attributed to local surface plasmon resonance induced by n-type doping<sup>[19,20]</sup>. The inset in Figure 2a schematically illustrates this mechanism. These findings confirm the strong infrared absorption capability of the ITO particles. To evaluate their photothermal conversion performance, ITO particles were embedded into PAm hydrogel films. As shown in Figure 2b, when exposed to an irradiation intensity of 200 mW cm<sup>-2</sup>, the temperature of the control film without ITO remained nearly unchanged, whereas the ITO-doped film exhibited a pronounced increase. Although photothermal conversion efficiency ( $\eta$ ) is a standard parameter for quantitatively assessing photothermal materials, the present study emphasizes the dual-responsive switching behavior enabled by ITO incorporation. The temperature evolution curves clearly demonstrate that doping with ITO particles leads to a rapid and substantial photothermal response compared with the pure hydrogel. Infrared thermal images of the films after 200 s of illumination are provided in Figure 2c.

Subsequently, thermosensitive PNIPAm microgels were synthesized. A characteristic feature of temperature-responsive PNIPAm hydrogels is that their optical scattering behavior is strongly influenced by particle size and internal structure. To ensure structural uniformity, PNIPAm microgels were prepared using a continuous feeding method. The synthesis process is illustrated in Figure 2d, where different feeding times were applied to control particle size. As shown in Figure 2e, particle size varied with feeding time, confirming that this method can reliably produce microgels of different dimensions. Optical microscopy of the sample obtained after 90 min revealed that the microgels were uniformly spherical, with an average diameter of approximately 1,300 nm (Figure S2).

Finally, ITO particles and PNIPAm microgels were incorporated into the PAm hydrogel film to construct the PPI composite film. The fabrication process is shown in Figure 2f. The chemical composition of the PAm-PNIPAm (P-P) hydrogel was verified by Fourier transform infrared (FTIR) spectroscopy (Figure 2g)<sup>[21-24]</sup>, confirming the successful synthesis of the targeted hydrogel. The integration of ITO particles and PNIPAm microgels into the PAm matrix produced a dual-responsive composite film with both thermally and optically driven modulation capabilities, thereby establishing the basis for subsequent performance evaluation.

# 3.2 Optimization of composite film performance

The first optimization step aimed to enhance  $\Delta T_{IR}$  by adjusting the size of the PNIPAm microgels. Microgels with particle sizes of 700 nm, 840 nm, 1,110 nm, and 1,365 nm were synthesized, and their transmittance was measured at 25 °C and 35 °C. As shown in Figure 3a, particle size decreased with increasing temperature, with the largest particles obtained at a feeding time of 90 min. The relationship between particle size and transmittance is further illustrated in Figure 3b,c.  $\Delta T_{IR}$  increased as particle size grew from 700 nm to 1,365 nm, reaching a maximum of 39.2% at 1,365 nm.

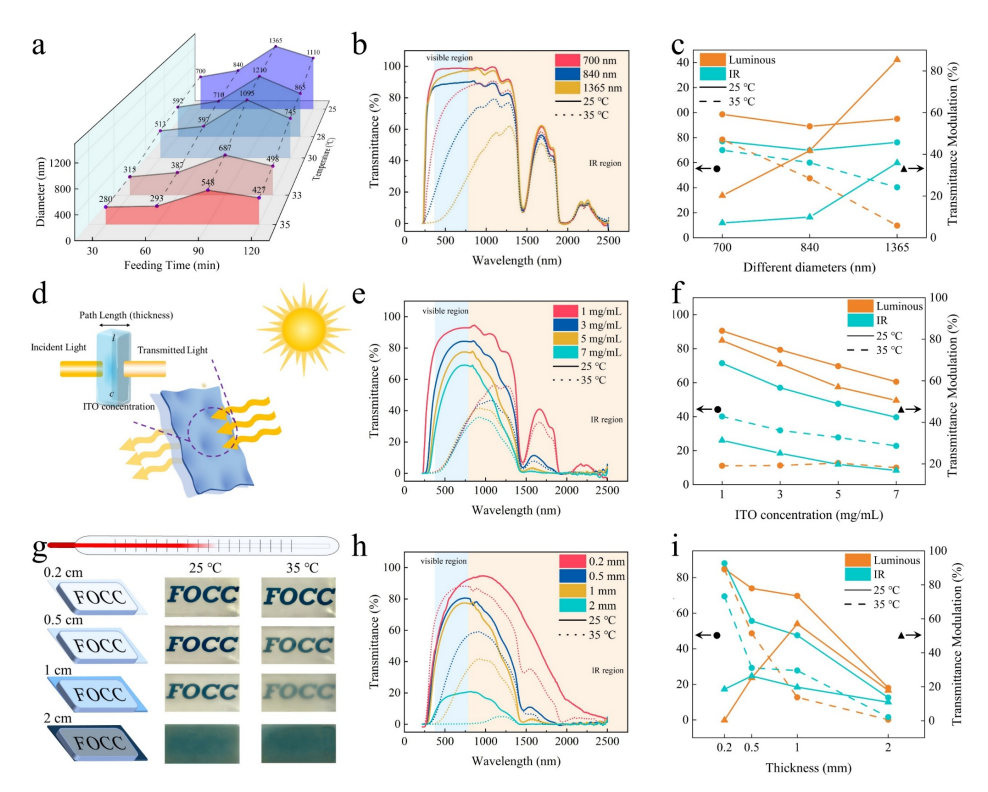


Figure 3. Performance optimization of PPI composite film. (a) Temperature-dependent diameter variation of microgels with different sizes; (b) UV-vis spectra of microgels with varying diameters at different temperatures; (c) Transmittance and modulation characteristics of microgels with varying diameters in the visible and infrared regions; (d) Schematic illustration of the effects of doping concentration and film thickness on performance; (e) UV-vis spectra of films with different doping concentrations at varying temperatures; (f) Transmittance and modulation characteristics of films with different doping concentrations in the visible and infrared regions; (g) Optical transparency of films with varying thicknesses in different thermochromic states; (h) UV-vis spectra of films with different thicknesses at varying temperatures; (i) Transmittance and modulation characteristics of films with different thicknesses in the visible and infrared regions. PPI: polyacrylamide/poly(N-isopropylacrylamide)/indium tin oxide.

This trend can be interpreted using Mie scattering theory, where the size parameter x is defined as [13]:

$$x = \frac{2\pi r}{\lambda} \tag{3}$$

where r is the particle radius and  $\lambda$  is the wavelength of the incident light. When the PNIPAm microgels are in the activated state, their x in the visible light region is approximately 1, resulting in low scattering efficiency in the infrared region. Effective infrared scattering occurs when the size parameter in the near-infrared (NIR) range approaches 1. For the 90 min sample, the particle diameter at 35 °C was 548 nm, yielding a size parameter in the infrared region close to 1, which explains the strongest  $\Delta T_{IR}$  response observed.

Next,  $\Delta T_{IR}$  was further improved by adjusting the doping concentration of ITO particles. According to the Beer-Lambert law<sup>[25]</sup>, absorbance is proportional to both the concentration of the absorbing species and the optical path length (Figure 3d). Due to the strong infrared reflectance of ITO particles, the  $\Delta T_{IR}$  of the PPI composite film increased as the ITO concentration increased. Figure 3e,f show the solar transmittance and its variation for the PPI composite film with doping concentrations of 1, 3, 5, and 7 mg/mL. At concentrations of 5 mg/mL and 7 mg/mL, the lowest  $T_{IR}$  values of 47.58% and 39.67%, respectively, were achieved. However, at 7 mg/mL,  $T_{lum}$  was markedly reduced, potentially compromising indoor illumination and visual comfort. In contrast, the composite film with an ITO concentration of 5 mg/mL achieved a substantial enhancement in  $\Delta T_{IR}$  while maintaining a  $T_{lum}$  of 69.73%, ensuring adequate visible-light transmission.

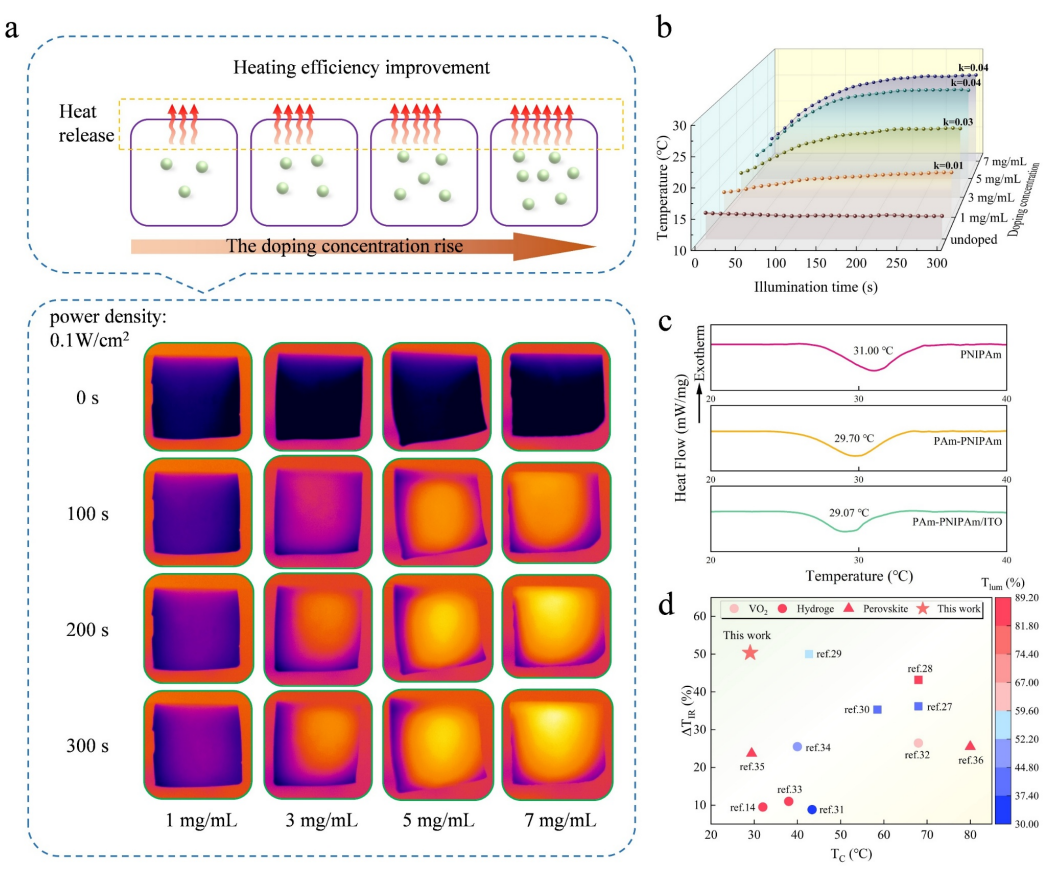
Having examined the factors governing infrared modulation, attention was then turned to  $T_{lum}$ , a parameter critical for both indoor brightness and external visibility. To address this, the film thickness was optimized to enhance  $T_{lum}$  in the activated state while maintaining sufficient  $\Delta T_{IR}$ . Composite films with thicknesses of 0.2mm, 0.5mm, 1mm, and 2mm were prepared. Transparency changes with temperature were qualitatively assessed by placing the films over a printed-text substrate (Figure 3g). The 2mm film exhibited complete opacity; therefore, only the 0.2mm, 0.5mm, and 1mm films were further evaluated.

Figure 3h,i present the solar transmittance and its variation for these three thicknesses. The 0.2mm film maintained high  $T_{lum}$  during the phase transition, but its  $\Delta T_{IR}$  was insufficient to meet performance requirements. The 0.5mm film achieved a well-balanced performance, with  $T_{lum}$  of 50% and  $\Delta T_{IR}$  of 50.4%. In contrast, the 1mm film caused a marked reduction in  $T_{lum}$  to 12.72%, falling short of the design target.

Through systematic adjustment of microgel particle size, ITO doping concentration, and film thickness, the PPI composite film achieved simultaneous enhancement of  $T_{lum}$  and  $\Delta T_{IR}$ , fulfilling the targeted performance objectives for dual-responsive smart window applications.

# 3.3 Optical switching and response temperature of the composite film

Following the identification of 5 mg/mL as the optimal ITO concentration, its impact on photothermal performance was further investigated. Figure 4a presents a schematic illustrating the effect of doping concentration on heating efficiency, accompanied by infrared thermal images of films irradiated at  $100 \text{ mW cm}^{-2}$  for the same duration. The complete set of thermographs is provided in Figure S3. It was observed that increasing the ITO concentration resulted in a more pronounced temperature rise. Figure 4b pshows the temperature–time curves of the composite films, with the heating rate k determined from the slope. The heating rate increased with ITO concentration, reaching a maximum at 5 mg/mL; beyond this point, k exhibited no further improvement, with both 5 mg/mL and 7 mg/mL yielding k = 0.04. However, the steady-state plateau temperature was slightly higher for the 7 mg/mL film. Considering the heating rate as a key photothermal parameter, these results confirm that 5 mg/mL is the optimal ITO concentration.



**Figure 4.** Optical switching behavior and  $T_C$  of the composite films. (a) Schematic illustration showing the effect of doping concentration on heating rate, along with infrared thermographs of films under equal illumination time at different doping concentrations; (b) Temperature evolution of films with varying doping concentrations under uniform illumination; (c) Critical transition temperatures of different samples; (d) Comparison of the performance of the present film with other reported smart windows, including  $VO_2^{(27-30)}$ , hydrogel<sup>[14,31-34]</sup>, and perovskite<sup>[35,36]</sup>.

The  $T_C$  values of the films are shown in Figure 4c. PNIPAm exhibited a  $T_C$  of 31 °C, consistent with literature values<sup>[26]</sup>. The P-P composite displayed a slightly lower TC than pure PNIPAm hydrogels, while incorporation of ITO particles did not substantially alter the  $T_C$ , which remained at 29.07 °C. Although DSC measurements are limited to assessing thermal switching under laboratory conditions, in practical applications, the synergistic effect of thermal and light-induced switching could significantly enhance the film's temperature control efficiency.

The combination of optimized thermochromic properties, high infrared modulation efficiency, and high  $T_{lum}$  provides a clear performance advantage over previously reported thermochromic systems, as illustrated in Figure 4d.

## 3.4 Application of the composite film

Following performance optimization, the thermal management capability and cycling stability of the PPI composite film were evaluated. Figure 5a shows a schematic of the experimental setup for assessing thermal management performance, with detailed device configurations provided in Figure S4. A thermocouple was used to monitor the internal temperature of the insulated chamber, enabling precise evaluation of the smart window's thermal regulation capability. A control experiment without the smart window film was conducted under identical conditions for comparison. During the tests, both the distance between the lamp and the building and the lamp intensity were kept constant.

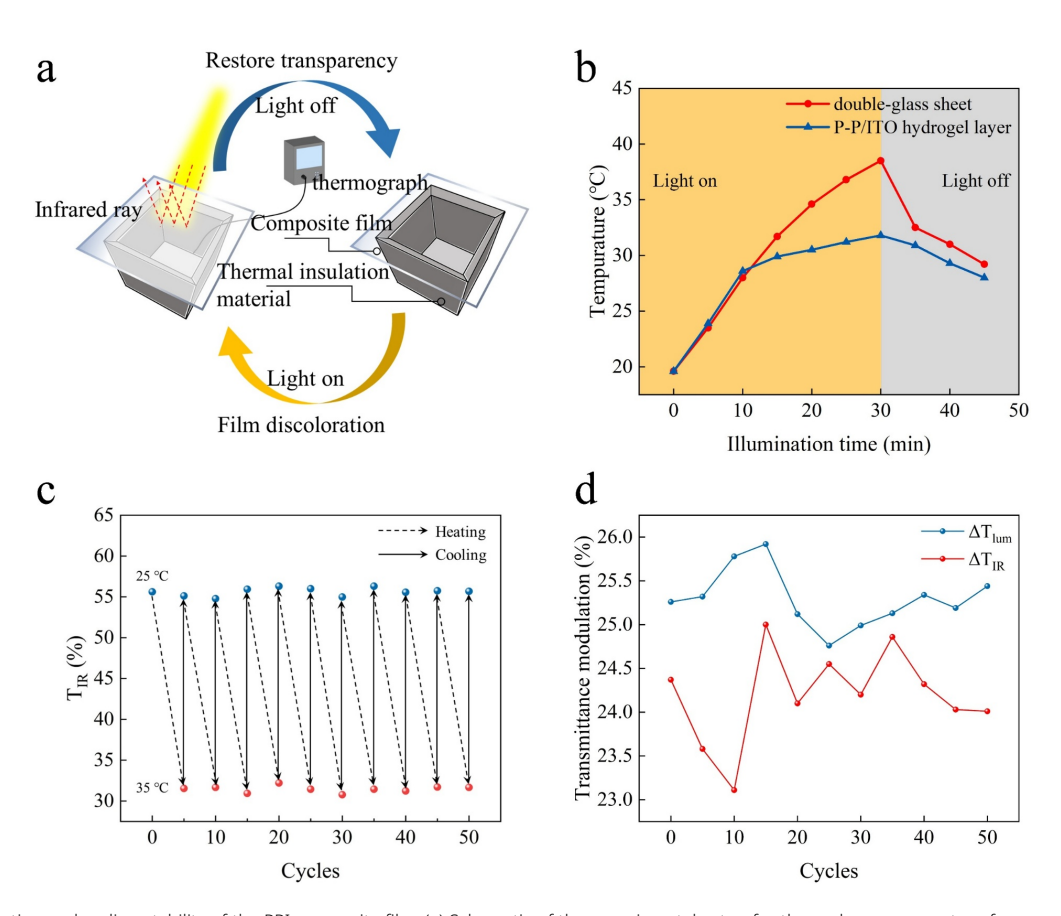


Figure 5. Application and cycling stability of the PPI composite film. (a) Schematic of the experimental setup for thermal management performance testing of the smart window device; (b) Temperature-time profile of the device during the thermal management experiment; (c, d) Cycling stability tests of the PPI composite film (1,365 nm, 5 mg/mL, 0.5 mm). PPI: polyacrylamide/poly(N-isopropylacrylamide)/indium tin oxide.

The experimental results are shown in Figure 5b. In the inactive state, the internal temperature of the building equipped with the PPI composite film increased more slowly under the same irradiation period. This behavior was attributed to the ITO particles embedded in the film, which effectively absorbed a portion of the incident infrared radiation and converted it into heat. Consequently, after 10min of illumination, the PPI composite film reached its TC and activated its thermal regulation function. This activation caused a clear divergence between the temperature profiles of the experimental and control samples. With continued illumination, the temperature of the control samples continued to rise, whereas that of the experimental samples stabilized, resulting in a maximum temperature difference of approximately 7 °C over the same illumination period. At this stage, the heating rates were 0.525 °C/min for the experimental samples and 0.16 °C/min for the control samples. These results highlight the significant potential of the fabricated hydrogel composite film for smart thermal management applications.

To assess durability, 50 consecutive heating–cooling cycles were performed, with the results presented in Figure 5c. The hydrogel composite film was encapsulated between two rigid glass substrates with a silicone sealing ring to minimize water loss and maintain stability under ambient conditions. Throughout the cycling test, the TIR of the composite film remained stable. Additionally,  $\Delta T_{lum}$  and  $\Delta T_{IR}$  were continuously monitored during the cycling tests. As shown in Figure 5d, both  $\Delta T_{lum}$  and  $\Delta T_{IR}$  exhibited no significant changes after cycling. These findings demonstrate the excellent cycling stability of the smart window film.

#### 4. Conclusion

In summary, a dual-responsive smart window film based on thermochromic PNIPAm was successfully developed and systematically characterized. The film exhibits large and broadband transmittance modulation, making it highly suitable for energy-efficient applications. Through precise control of PNIPAm microgel particle size, combined with the incorporation of ITO particles into the polymer matrix, the PPI composite film achieves a substantial enhancement inn  $\Delta T_{IR}$ , increasing from 39.2% to 50.4% compared with the pure PNIPAm hydrogel. Furthermore, the film demonstrates a high  $T_{lum}$  of 50% in the activated state and a low  $T_C$  of 29 °C. Application of the PPI composite film is expected to reduce indoor temperatures by up to 7 °C, while maintaining excellent stability and scalability, highlighting its practical potential. This design strategy and the obtained results demonstrate that dynamic modulation of transmittance in smart window materials is an effective approach toward real-world applications. Overall, this work provides a promising and scalable platform for the development of next-generation smart windows, combining high optical performance with practical durability. By enabling effective thermal and optical control, it contributes a valuable design strategy for sustainable architecture and energy-efficient technologies.

# Supplementary materials

The supplementary material for this article is available at: Supplementary materials.

#### **Declarations**

# Acknowledgements

Qi Wang acknowledges the support from the start-up funding of the Suzhou Institute for Advanced Research at the University of Science and Technology of China. Weidong Zheng acknowledges the support from Natural Science Foundation of Shandong Province and the Taishan Scholars Program of Shandong Province.

### **Authors contribution**

Jianq Z: Article conception, methodology design, experiments, data analysis, and manuscript writing.

Yang Y: Supervision, initial draft review, and critical revision.

Feng W: Funding acquisition, overall project supervision, and final approval of the manuscript.

Li Y: Assistance with experimental procedures and data collection.

Peng C: Support with data interpretation and figure preparation.

## **Conflict of interest**

Wei Feng is an Editorial Member of *Thermo-X*. The other authors declare no conflicts of interest.

# **Ethical approval**

Not applicable.

# Consent to participate

Not applicable.

#### Consent for publication

Not applicable.

## Availability of data and materials

The data that support the findings of this study are available from the corresponding author upon reasonable request.

# **Funding**

This work was financially supported by the National Key R&D Program of China (Grant No.2022YFB3805702) and the National Natural Science Foundation of China (Grant Nos. 52130303 and 52327802).

# Copyright

© The Author(s) 2025.

#### References

- 1. Ma R, Li D, Xu C, Yang J, Huang J, Guo Z. Fabricated advanced textile for personal thermal management, intelligent health monitoring and energy harvesting. Adv Colloid Interface Sci. 2024;332:103252. [DOI]
- 2. Vilà R, Martorell I, Medrano M, Castell A. Adaptive covers for combined radiative cooling and solar heating. A review of existing technology and materials. Sol Energy Mater Sol Cells. 2021;230:111275. [DOI]
- 3. Xie L, Wang X, Bai Y, Zou X, Liu X. Fast-developing dynamic radiative thermal management: full-scale fundamentals, switching methods, applications, and challenges. Nano-Micro Lett. 2025;17(1):146. [DOI]
- 4. Yu D, Zhuo S, Wang J, Liu Z, Ye J, Wang Y, et al. Thermochromic Ni(II) organometallics with high optical transparency and low phase-transition temperature for energy-saving smart windows. Small. 2023;19(22):2205833. [DOI]
- 5. Xu Z, Zhang C, Wang F, Yu J, Yang G, Surmenev RA, et al. Smart textiles for personalized sports and healthcare. Nano-Micro Lett. 2025;17(1):232. [DOI]
- 6. Zhuo S, Zhao YD, Liu YX, Rong Y, Ju YY, Gu LF, et al. Radical-activable charge-transfer cocrystals for solar thermoelectric generator toward information conversion. Natl Sci Rev. 2025;12(5):nwaf121. [DOI]
- 7. Feng M, Bu X, Yang J, Li D, Zhang Z, Dai Y, et al. Review: smart windows based on photonic crystals. J Mater Sci. 2020;55(20):8444-8463. [DOI]
- 8. Hoon Lee J, Jeong J, Tae Chae Y. Optimal control parameter for electrochromic glazing operation in commercial buildings under different climatic conditions. Appl Energy. 2020;260:114338. [DOI]
- 9. Zhao Z, Liu Y, Wang D, Ling C, Chang Q, Li J, et al. Sn dopants improve the visible transmittance of VO<sub>2</sub> films achieving excellent thermochromic performance for smart window. Sol Energy Mater Sol Cells. 2020;209:110443. [DOI]
- 10. Zhou Y, Wang S, Peng J, Tan Y, Li C, Boey FY, et al. Liquid thermo-responsive smart window derived from hydrogel. Joule. 2020;4(11):2458-2474. [DOI]
- 11. Fang Z, Ding L, Li L, Shuai K, Cao B, Zhong Y, et al. hermal homeostasis enabled by dynamically regulating the passive radiative cooling and solar heating based on a thermochromic hydrogel. ACS Photonics. 2021;8(9):2781-2790. [DOI]
- 12. Ube T, Imai J, Yoshida M, Fujisawa T, Hasebe H, Takatsu H, et al. Sunlight-driven smart windows with polymer/liquid crystal composites for autonomous control of optical properties. J Mater Chem C. 2022;10(35):12789-12794. [DOI]
- 13. Li XH, Liu C, Feng SP, Fang NX. Broadband light management with thermochromic hydrogel microparticles for smart windows. Joule. 2019;3(1):290-302. [DOI]
- 14. Zhou Y, Cai Y, Hu X, Long Y. Temperature-responsive hydrogel with ultra-large solar modulation and high luminous transmission for "smart window" applications. J Mater Chem A. 2014;2(33):13550-13555. [DOI]
- 15. Yang Z, Zhang M, Zhao X, Hu R, Zhao H, Zeb S, et al. Fluorine-doped ATO NCs with enhanced LSPR effect for smart windows with adaptive solar modulation. Ceram Int. 2024;50(11):19543-19551. [DOI]
- 16. Feng B, Yang T, Zhu S, Yue Y, Zhou B, Yao Z, et al. Flexible, highly transparent, and conductive ITO/Ag/ITO film with double symmetric structure for electrical heater and broadband electromagnetic interference shielding. Chem Eng J. 2025;516:164233. [DOI]
- 17. Wang S, Liang K, Zhao H, Wu M, He J, Wei P, et al. Electronic structure formed by Y<sub>2</sub>O<sub>3</sub>-doping in lithium position assists improvement of charging-voltage for high-nickel cathodes. Nat Commun. 2025;16(1):1. [DOI]
- 18. Ali A, Jeon D, Kim W, Hoang VQ, Lee J, Son DH, et al. Highly efficient bifacial narrow bandgap Ag-CuInSe<sub>2</sub> solar cells on ITO. Adv Energy Mater. 2025;15(23):2500899. [DOI]
- 19. Guo J, Hou J, Wan Y, Yang Z, Li Y, Zhu Y, et al. Integrating thermal vibration and local surface plasmon resonance effect boosted "Symbiotic Co-evolution" for efficient solar evaporation, antimicrobial and antibiotic resistance genes removal. Water Res. 2025;284:123997. [DOI]
- 20. Wang Y, Zhao R, Xu Y, Sun B, Zhou Z, Yu P, et al. S-Pt coordination bond enhanced local surface plasmon resonance boosts photocatalytic H<sub>2</sub> production coupled with high value-added products from plastic waste. Nano Energy. 2025;141:111103. [DOI]
- 21. He D, Zhu T, Sun M, Chen J, Luo H, Li J. Unraveling synergistic mechanisms of polyacrylamide coagulation and Fe<sup>2+</sup>/CaO<sub>2</sub> Fenton-like oxidation to enhance sludge dewatering. Chem Eng J. 2024;479:147576. [DOI]
- 22. Wang F, Yu X, Cao Z, Liu Y, Jiang X, Gu X. Synergic enhancement of hydrogel upon multi-level hydrogen bonds via macromolecular design for dual-mode electronic skin. Chem Eng J. 2024;489:151249. [DOI]
- 23. Lee S, Moon S, Ok Y, Lee Y, Park Y. Magnetically recoverable nanoparticle organic hybrid materials as kinetic hydrate inhibitors. Chem Eng J. 2024;501:157612. [DOI]
- 24. Bardajee GR, Mahmoodian H, Mahmoudi N, Felegari N, Rouhi M. Disulfide-crosslinked PNIPAM nanogels for efficient removal of copper and cadmium ions from aqueous solutions. J Environ Chem Eng. 2025;13(5):117473. [DOI]
- 25. Walter AD, Schwenk GR, Liu Y, Bugallo Ferron D, Wilk JT, et al. Concentration-dependent control of the band gap energy of a low-dimensional lepidocrocite titanate. ACS Nano. 2025;19(4):4855-4866. [DOI]
- 26. Li BY, Lin TY, Lai YJ, Chiu TH, Yeh YC. Engineering multiresponsive alginate/PNIPAM/carbon nanotube nanocomposite hydrogels as on-

- demand drug delivery platforms. Small. 2025;21(12):2407420. [DOI]
- 27. Kang L, Gao Y, Chen Z, Du J, Zhang Z, Luo H.  $Pt/VO_2$  double-layered films combining thermochromic properties with low emissivity. Sol Energy Mater Sol Cells. 2010;94(12):2078-2084. [DOI]
- 28. Zhang Z, Gao Y, Chen Z, Du J, Cao C, Kang L, et al. Thermochromic VO<sub>2</sub> thin films: solution-based processing, improved optical properties, and lowered phase transformation temperature. Langmuir. 2010;26(13):10738-10744. [DOI]
- 29. Du J, Gao Y, Chen Z, Kang L, Zhang Z, Luo H. Enhancing thermochromic performance of VO<sub>2</sub> films via increased microroughness by phase separation. Sol Energy Mater Sol Cells. 2013;110:1-7. [DOI]
- 30. Zhu J, Huang A, Ma H, Yining M, Kun T, Shidong J, et al. Composite film of vanadium dioxide nanoparticles and ionic liquid-nickel-chlorine complexes with excellent visible thermochromic performance. ACS Appl Mater Interfaces. 2016;8(43):29742-29748. [DOI]
- 31. Lee HY, Cai Y, Bi S, Liang YN, Song Y, Hu XM. A dual-responsive nanocomposite toward climate-adaptable solar modulation for energy-saving smart windows. ACS Appl Mater Interfaces. 2017;9(7):6054-6063. [DOI]
- 32. Zhou Y, Cai Y, Hu X, Long Y. VO<sub>2</sub> /hydrogel hybrid nanothermochromic material with ultra-high solar modulation and luminous transmission. J Mater Chem A. 2015;3(3):1121-1126. [DOI]
- 33. Yang YS, Zhou Y, Yin Chiang FB, Long Y. Temperature-responsive hydroxypropylcellulose based thermochromic material and its smart window application. RSC Adv. 2016;6(66):61449-61453. [DOI]
- 34. Cao D, Xu C, Lu W, Qin C, Cheng S. Sunlight-driven photo-thermochromic smart windows. Sol Rrl. 2018;2(4):1700219. [DOI]
- 35. Liu S, Du YW, Tso CY, Lee HH, Cheng R, Feng SP, et al. Organic hybrid perovskite (MAPbI $_{3^-x}$ Cl $_x$ ) for thermochromic smart window with strong optical regulation ability, low transition temperature, and narrow hysteresis width. Adv Funct Mater. 2021;31(26):2010426. [DOI]
- 36. Zhang Y, Tso CY, Iñigo JS, Liu S, Miyazaki H, Chao CY, et al. Perovskite thermochromic smart window: advanced optical properties and low transition temperature. Appl Energy. 2019;254:113690. [DOI]

# **Publisher's Note**

Science Exploration remains a neutral stance on jurisdictional claims in published maps and institutional affiliations. The views expressed in this article are solely those of the author(s) and do not reflect the opinions of the Editors or the publisher.